Korean J. Chem. Eng., 34(6), 1651-1660 (2017)
DOI: 10.1007/s11814-016-0329-6

pISSN: 0256-1115
eISSN: 1975-7220

Perovskite-type $LaFe_{1-x}Mn_xO_3$ (x=0, 0.3, 0.5, 0.7, 1.0) oxygen carriers for chemical-looping steam methane reforming: Oxidation activity and resistance to carbon formation

Kun Zhao*,,***, Fang He*,†, Zhen Huang*, Guoqiang Wei*, Anqing Zheng*, Haibin Li*, and Zengli Zhao***

*Key Laboratory of Renewable Energy, Chinese Academy of Sciences,
Guangdong Key Laboratory of New and Renewable Energy Research and Development,
Guangzhou Institute of Energy Conversion, Chinese Academy of Sciences, Guangzhou 510640, China
**University of Chinese Academy of Sciences, Beijing 100049, China
***Key Laboratory of Energy Thermal Conversion and Control of Ministry of Education,
Southeast University, Nanjing 210096, China
(*Received 26 August 2016 • accepted 20 November 2016*)

Abstract−The effects of Mn substitution of $LaMn_xFe_{1-x}O_3$ (x=0, 0.3, 0.5, 0.7, 1.0) on the oxidation activity and resistance to carbon formation for chemical-looping steam methane reforming (CL-SMR) were investigated. The desired crystalline perovskite phases were formed by transferring from the orthorhombic structure of $LaFeO_3$ to rhombohedral lattice of $LaMnO_3$ as the degree of Mn-doping increased. Manganese ions have a mixed state of Mn^{3+} and Mn^{4+} in the $LaFe_{1-x}Mn_xO_3$, meanwhile inducing the states of highly mixed character of Fe^{2+}, Fe^{3+} and Fe^{4+} in iron ions. Substitution of Mn for Fe with proper value not only increases the lattice oxygen, which is conducive to the partial oxidation of CH_4 to produce syngas, but also enhances the lattice oxygen mobility from the bulk to the surface of the oxygen carrier particles. Judging from the points of the redox reactivity, resistance to carbon formation and hydrogen generation capacity, the optimal range of the degree of Mn substitution is x=0.3-0.5.

Keywords: Perovskite, CL-SMR, Manganese, Carbon Formation, Hydrogen

INTRODUCTION

Conversion of methane to syngas (H_2+CO) by using lattice oxygen of solid oxygen carriers is a creative technology for the conversion of methane [1,2]. Chemical-looping steam methane reforming (CL-SMR) [3] is a further development based on this technology for the cooperative production of syngas and hydrogen by using three reactors, as shown in Fig. 1. Partial oxidation of methane to syngas happens in the fuel reactor with oxygen carrier, and then the steam oxidation reaction takes place on the reduced oxygen carrier to recover its partial lattice oxygen; meanwhile pure hydrogen is generated. An air reactor is also needed for complete recovery of the lattice oxygen. In CL-SMR, syngas and hydrogen can be, respectively, produced via two steps. Since there is no direct contact between methane and gaseous molecular oxygen, the risk of CH_4 explosion can be avoided. Meanwhile, additional gas treatments and separation processes are not needed in the steam oxidation stage.

The success of CL-SMR mainly depends on the oxygen carrier with the following properties [4]: (i) excellent oxygen storage and transport capacity; (ii) good redox reactivity in the reduction and oxidation cycles; (iii) ability to selectively oxidize methane; and (iv) resistance to agglomeration and carbon formation. Thanks to the high oxygen storage capacity, good mechanical properties and favorable reactivity, perovskite-type oxides are ideal candidates as the oxygen carriers for CL-SMR. Perovskite-structured oxides are a kind of mixed oxides with the form of ABO_3, where A is an alkaline earth metal and B is a transition metal ion. Dai et al. [5] chose $LaFeO_3$ as catalysts for methane selectively oxidization. It was found that $LaFeO_3$ oxide exhibited the best performance for syngas pro-

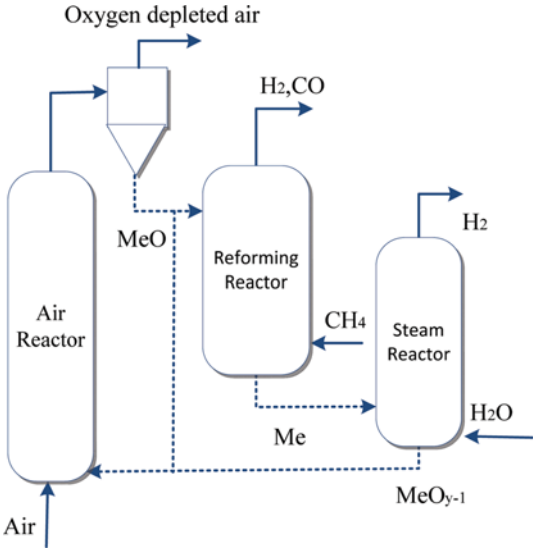

Fig. 1. CL-SMR for syngas and hydrogen production.

†To whom correspondence should be addressed.
E-mail: hefang@ms.giec.ac.cn

duction compared with that of $NdFeO_3$ and $EuFeO_3$. Substituted perovskite-type oxides derived from $LaFeO_3$, e.g., partial substitution of La^{3+} by Sr^{2+} and Ce^{2+}, also have been extensively studied [6-8]. The catalytic activity and diffusion of lattice oxygen can be highly improved by selectively substitution on A-sites cations. But the carbon formation caused by methane cracking is inevitable in the methane reforming reactions. While the substitution of B-site cations is studied less. That may be because the ion radius of transition metal in B site does not appear to be much different from each other; therefore, the ion radius effect and valence effect, which are aroused by B-site element, are not obvious. Actually, B-site is the essential active site in perovskite-type oxides. When the valence states of A-site metals change, the electron orbit of B-site metals will be adjusted to adapt to the environmental changes. García [9] used the temperature-programmed surface reaction of methane and pulses reaction to study the $BaTi_{1-x}In_xO_3$ perovskite oxides with nickel as a catalyst for methane oxidation. They found that the reducibility of B cation strongly influenced the activity and selectivity of oxygen carriers. Nalbandian [10] used $La_{1-x}Sr_xM_yFe_{1-y}O_{3-\delta}$ (M=Ni, Co, Cr, Cu) as oxygen carriers for methane chemical looping reforming. They found that the change of B-site metals had an obvious effect on the performance of oxygen carrier both in the fuel oxidation step and in water splitting step. Neal [11] investigated a core-shell catalyst Fe_2O_3@$La_{0.8}Sr_{0.2}FeO_{3-\delta}$ for methane partial oxidation. The core-shell materials have the promise to provide higher selectivity for methane conversion with lower solid circulation rates than traditional redox catalysts. Lim [12] introduced a perovskite catalytic particle of Fe_2O_3-NiO/$La_{0.8}Sr_{0.2}FeO_3$ as an oxygen carrier and investigated its long-term activity and stability in a novel methane chemical looping reforming decomposition process.

As an easily available and reasonably environmentally benign transition metal, manganese ion (Mn) exists in a remarkably high number of oxidation states from Mn^{2+} to Mn^{7+}. Combinations of Mn with other cheap and harmless materials are highly attractive with expansive researching spaces [13]. Azimi [14] investigated the combination of iron and manganese oxides for the chemical-looping with oxygen uncoupling (CLOU) process. Results showed that higher manganese content is disadvantageous for oxygen release ascribed to the failure formation of bixbyite, and 25% to 33% ranges of manganese content in the iron-manganese oxides give the best gas conversion of methane at 950 °C. Wei [15] used $La_{1-x}Sr_xMO_3$ (M=Mn, Ni) and $LaMnO_{3-\alpha}F_\beta$ perovskite oxides for the partial oxidation of methane to produce synthesis gas. They concluded that the B-site metals influence the stability of the perovskite structure and the selectivity of lattice oxygen. So far as we know, there are fewer researches on the perovskite-type oxide $LaMn_xFe_{1-x}O_3$ as an oxygen carrier for CL-SMR.

In this work, $LaFe_{1-x}Mn_xO_3$ (x=0, 0.3, 0.5, 0.7, 1.0) perovskite-type metal oxides were prepared by combustion method. X-ray diffraction (XRD), H_2 temperature-programmed reduction (H_2-TPR), and X-ray photoelectron spectroscopy (XPS) technologies were used to characterize the properties of the perovskites. Then the oxidation activity and resistance to carbon formation of the oxygen carriers was investigated in a TGA and a fixed-bed reactor to examine the influence of substitution of Mn on the characteristics of the $LaFe_{1-x}Mn_xO_3$. The optimal substitution value of Mn in the oxides $LaFe_{1-x}Mn_xO_3$ was determined by meeting the requirements of high CH_4 conversion, suitable H_2/CO molar ratio and high hydrogen generation capacity.

EXPERIMENTAL SECTION

1. Synthesis of $LaMn_xFe_{1-x}O_3$

The perovskite-type oxides $LaFe_{1-x}Mn_xO_3$ (x=0, 0.3, 0.5, 0.7, 1.0) were synthesized by glycine combustion method. $La(NO_3)_3{\cdot}6H_2O$, $Fe(NO_3)_3{\cdot}9H_2O$ powder reference samples with 99.99% purity, and $Mn(NO_3)_2$ solution with 50 wt% in H_2O were purchased from Aladdin. $La(NO_3)_3{\cdot}6H_2O$, $Fe(NO_3)_3{\cdot}9H_2O$ and $Mn(NO_3)_2$ with at a desired stoichiometric ratio of 0.1 mol were dispersed in deionized water to make a precursors solution. The nitrate ions serve as oxidant during the combustion process. Glycine solution was added into the solution of the mixed nitrates to reach a glycine/nitrates molar ratio of 1.05, which acts as the fuel in the combustion process. After the evaporation process at 70 °C, the obtained viscous gel was then put in a muffle furnace for combustion at 250 °C for 30 min. Finally, the powdered precursor was calcined at 900 °C for 6 h and ground to 80-100 mesh particle size.

2. Sample Characterizations

XRD was performed by using a PANalytical X'Pert Pro XRD system with a Cu Kα radiation (λ=0.15406 nm) operated at 40 kV with a current of 40 mA which confirmed the rhombohedral and orthorhombic structures for both synthesized samples. The diffraction angle (2θ) was scanned from 10° to 80°. Hydrogen-temperature programmed reduction (H_2-TPR) experiments were used to test the reducibility of oxygen carriers. Perovskite-type oxides were put in a U-tube and reacted with H_2 (5.0 vol% balanced with helium) at a flow rate of 60 ml/min. The temperature program was raised from room temperature to 800 °C with a heating rate of 10 °C/min. X-ray photoelectron spectroscopy (XPS) was used to probe the near-surface composition of the oxides. The Thermo Fisher Scientific Inc equipment was comprised of an Al Kα X-ray source. Survey spectra and narrow scan spectra were taken with pass energy of 20 eV and 100 eV, respectively.

3. Reactivity Test

Redox reactivity of $LaFe_{1-x}Mn_xO_3$ was conducted in a TGA reactor [16]. The oxygen carriers were exposed to alternating methane and air conditions multi-circularly. To put it simply, the sample was placed on the quartz pan suspended by a thin stainless wire hung from the electric microbalance. A computer that connected with the microbalance was used to record the weight change of the oxides. The redox experiments were performed at 850 °C, then 40% CH_4 balance N_2 and dry air were alternately introduced into the reaction tube.

The oxidation degree X was introduced to evaluate the reactivity of oxygen carrier in thermogravimetric analysis:

$$X = \frac{m - m_{red}}{m_{ox} - m_{red}} \quad (1)$$

where m is the weight of oxygen carrier measured by microbalance; m_{red} is the weight of oxygen carrier after reduction; and m_{ox} is the weight of oxygen carrier when fully oxidized.

CL-SMR experiment was carried out in a fixed-bed quartz reac-

tor, as shown detailed in our previous research [17]. The temperature of reaction also settled at 850 °C. The redox experiments were performed in 40% CH_4 balance N_2, steam and dry air, respectively. Pure N_2 was introduced to the reactor during the two steps to be a purge gas. Then the collected gases using gas bags were analyzed by a gas chromatograph (Shimadzu GC-2010 plus).

RESULTS AND DISCUSSION

1. Characterization of $LaFe_{1-x}Mn_xO_3$

1-1. XRD

The structures of $LaFe_{1-x}Mn_xO_3$ (x=0, 0.3, 0.5, 0.7, 1.0) perovskites were examined by XRD as shown in Fig. 2(a)-(d), respectively. It can be seen from Fig. 2(a) that the five XRD patterns are in good agreement with JCPDS (Joint Committee on Powder Diffraction Standards) card 01-088-0641, confirming the formation of the desired monophasic crystalline perovskites. Peaks corresponding to iron oxides, lanthanum oxides and manganese oxides are not observed, indicating the incorporation of Mn with Fe in perovskite structure. The orthorhombic perovskite structure was obtained for $LaFeO_3$ ($LaMn_xFe_{1-x}O_3$, x=0), while the cubic crystal system was formed for the samples with x=0.3 and x=0.5. As the Mn substitution increased continuously, the perovskite structure turned to rhombohedral for the samples with x=0.7 and x=1.0. The peak splitting at about 2θ=32.2°, 39.6°, 46.2°, 57.5° and 67.4° was observed for the samples with x=0.5, 0.7 and 1.0, indicating the formation of mixed crystal phase. As the degree of Mn substitution increased, a slight shifting towards higher 2θ was observed, indicating the decrease in crystal interplanar distance, which was caused by the lattice distortion. Although the ion radius of Mn (r_{Mn}= 1.79 Å) is larger than that of Fe (r_{Fe}=1.72 Å) [18], the difference ion radius of Mn and Fe is so tiny that it cannot counter the compressed stress, which leads to the shrinking of crystal size. These results were also observed by Sheenu [19] who discussed the catalytic activity of Mn-doped lanthanum ferrites in the presence and absence of visible light irradiation. Fig. 2(b) shows the reduced samples after removal of oxygen during methane reduction. The perovskite structures still exist with formation a few of impurity phases. To discuss the reduced samples in detail, the XRD pattern of reduced sample $LaFe_{0.7}Mn_{0.3}O_3$ is taken for an example as shown in Fig. 2(c). The characteristic peaks of La_2O_3 are observed obviously in the structure of the reduced sample, indicating that part of La^{3+} separates out from the perovskite structure and appears in the form of La_2O_3. In addition, Fe-based oxide or Mn-based oxide was not found after the methane reduction, attributed to the incorporation of Fe ion and Mn ion in the perovskite structure. The perovskite structures do not break up after methane reduction. Fig. 2(d) shows the XRD patterns of regenerated oxides after five redox reactions; all the regenerated oxides recover to the original perovskite structure with good regenerability.

1-2. H_2-TPR

H_2-TPR experiments were performed to study the reducibility

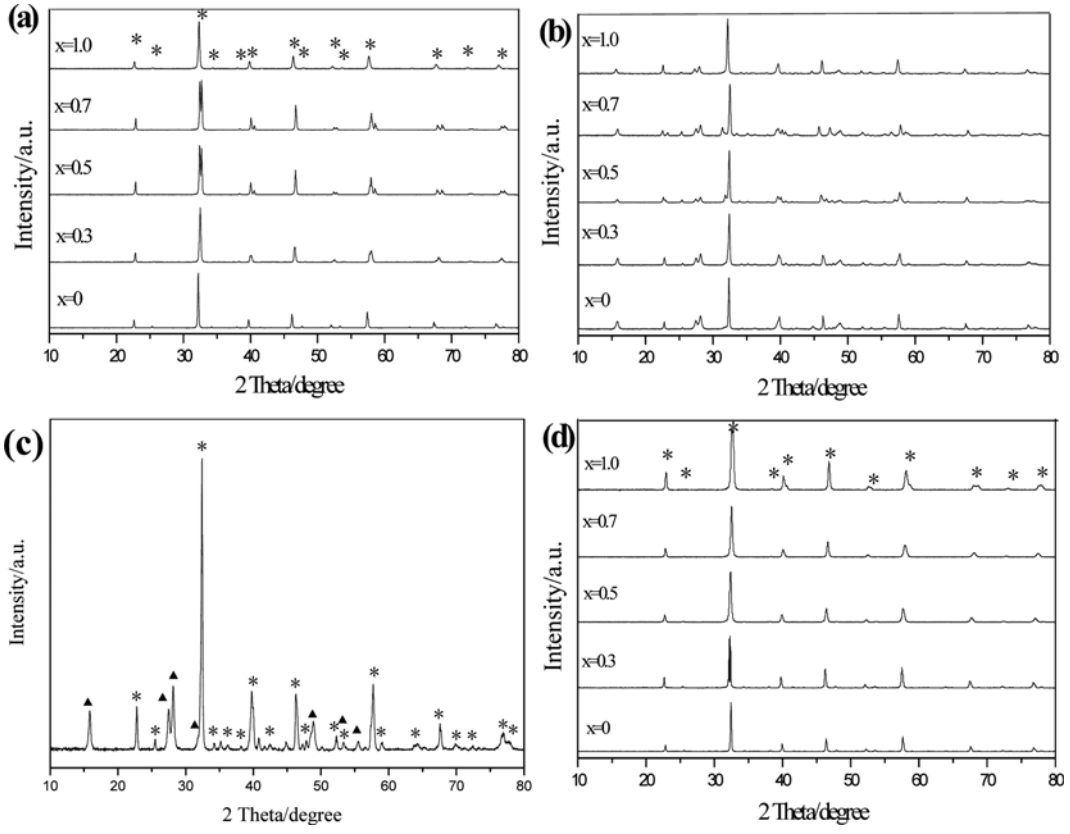

Fig. 2. XRD patterns of $LaFe_{1-x}Mn_xO_3$ perovskites. (a) Fresh, (b) reduced, (c) reduced $LaFe_{0.3}Mn_{0.7}O_3$ and (d) after five redox reactions (* perovskite, ▲ La_2O_3).

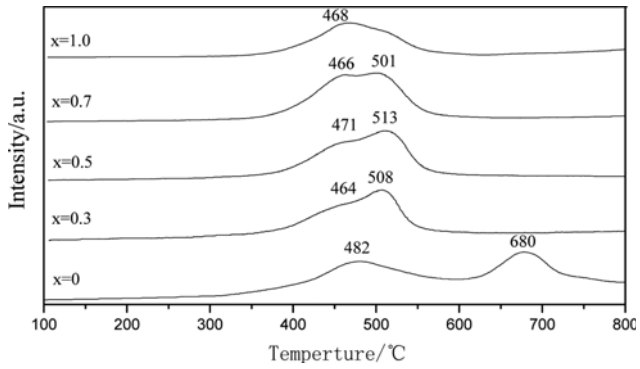

Fig. 3. H_2-TPR profiles of oxygen carriers.

Table 1. Hydrogen consumption of five perovskites

Oxygen carriers ($LaMn_xFe_{1-x}O_3$)	Peak position (°C)	H_2 consumption (mol per mol oxygen carrier)
x=0	482, 680	0.0613
x=0.3	464, 608	0.0201
x=0.5	471, 513	0.0287
x=0.7	466, 501	0.0332
x=1.0	468	0.0346

of $LaFe_{1-x}Mn_xO_3$ perovskite-type oxides. In Fig. 3, the TPR profile of $LaFeO_3$ features two peaks at 482 °C and 680 °C. While for the sample with Mn doping, the TPR profiles of $LaFe_{1-x}Mn_xO_3$ (x= 0.3, 0.5, 0.7, 1.0) present a broad band instead of two well-defined peaks, with an inconspicuous peak shoulder. A reduction peak with a defined maximum at 508 °C is shown for the sample $LaFe_{0.7}Mn_{0.3}O_3$. When the substitution value x increases to 0.5, the reduction peak becomes broader and shifts to higher temperatures to 513 °C. The sample of x=0.7 shows the broadest hydrogen consumption peak

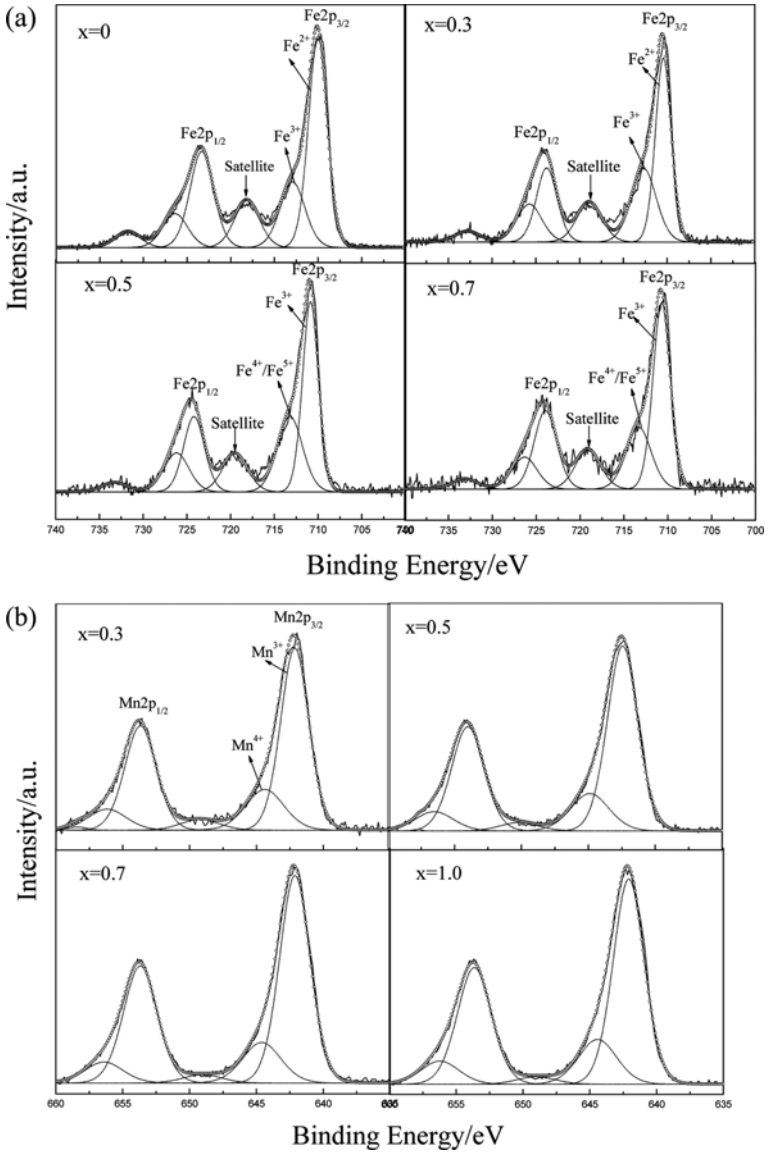

Fig. 4. XPS spectra of $LaFe_{1-x}Mn_xO_3$ perovskites. (a) Fe2p, (b) Mn2p.

starting at 466 °C and with a maximum at 501 °C. When the Mn substitution increases to 1.0, the TPR curve of $LaMnO_3$ shows a sharp reduction peak at 466 °C without peak shoulder. Generally, there are two kinds of oxygen species in perovskite-type oxide: The first is the surface adsorbed oxygen which can be reduced at low temperature; second is the lattice oxygen which is presented at high temperature and associated with the reduction of B-site cations. The emergence of single reduction peak for $LaFe_{1-x}Mn_xO_3$ (x=0.3, 0.5, 0.7, 1.0) indicates the simultaneous reduction of surface oxygen and lattice oxygen without clear distinction [20]. It means that the oxygen located in the bulk of the oxide could come to the surface rapidly as the surface oxygen is consumed, representing good oxygen mobility. Besides, the reduction peak area that represents the hydrogen consumption increase as the degree of Mn substitution increases, as shown in Table 1.

1-3. XPS

XPS technology was used to explore the further information with respect to the surface properties. Since the catalytic activity of perovskite-type oxide is mainly determined by the B-site metals, the valence states of Fe and Mn play important roles in the reactivity of perovskites. The chemical states of metals Fe and Mn are given by fitting the XPS curves as shown in Fig. 4. Smart-type algorithm was used to model the background, and Gauss-Lorentz line shape was used to fitting the peak shape. The elemental compositions as well as the relative proportions were calculated on basis of the XPS data as summarized in Table 1.

Both the XPS patterns of Fe2p and Mn2p exhibit an asymmetry feature with double-peaked spectrum, accompanied with satellite peaks. It's the feature of the existence of multiple components of Fe or Mn with different chemical valence states in an oxide environment. The peak positions of $Fe2p_{3/2}$ for the two samples with x=0 and 0.3 are located at 709.6-710.8 eV, which is typical of Fe ions in high oxidation states attributed to both of Fe^{2+} and Fe^{3+} oxidation states. When the substitution value x increases to 0.5 and 0.7, the peak positions of $Fe2p_{3/2}$ shift to high binding energy to higher than 710.8 eV, which means that the chemical valence states of Fe turn to Fe^{3+} and Fe^{4+}. Mn substitution induces the states of highly mixed character of Fe^{2+}, Fe^{3+} and Fe^{4+} in iron ions. As the substitution value of Mn increases to 0.5 and 0.7, a higher amount of Fe^{4+} ions may be generated to compensate the charge unbalance. Due to the unstable property of Fe^{4+}, however, Fe^{3+} ions are still the primary components for all the samples.

Previous research has shown that many stable oxidation states of Mn ions existed, ranging from 0 to +7 [21], and Mn^{2+}, Mn^{3+} and Mn^{4+} are the common valence states of Mn in perovskite-type oxides [22]. Therefore, it is a challenge to fit the Mn ions, in comparison to the case of Fe ions. In Fig. 4(b), the XPS patterns of Mn2p exhibit asymmetric features, which are caused by the change of valence state from Mn^{3+} to Mn^{4+}. And the satellite peak representing the reduced Mn^{2+} state does not show up in the spectrum. Therefore, the manganese ions have a mixed state of Mn^{3+} and Mn^{4+}, which was also confirmed by Tabata [22]. A fraction of Mn^{4+} decreases with the increase of Mn substitution from x=0.3 to x=0.7, except for the sample $LaMnO_3$. And Mn^{3+} is the dominating valence state of Mn ions in $LaMn_xFe_{1-x}O_3$.

Fig. 5 shows the chemical states of oxygen by fitting the XPS

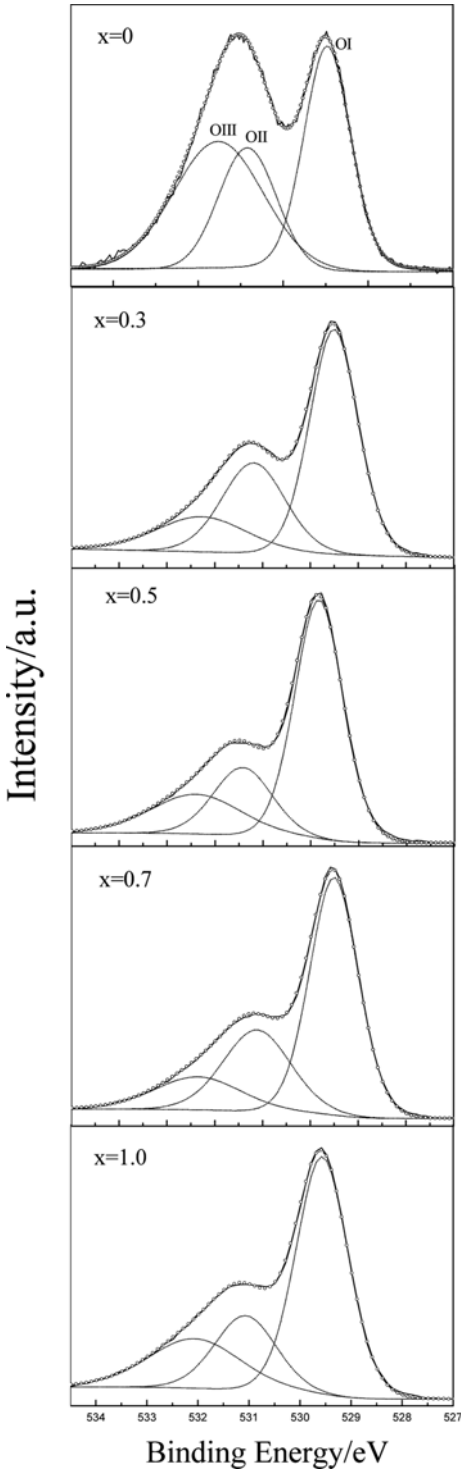

Fig. 5. XPS deconvolution spectra of O1s peak.

curves using three peaks that represent three kinds of oxygen species. The first is the lattice oxygen at 528.3-529 eV (denoted as OI), the second is the chemisorbed oxygen at 530.5-530.9 eV (denoted as OII), and the third is the physical adsorbed oxygen at 531.5-531.7 eV (denoted as OIII), respectively [23]. As can be seen form Table 2, the lattice oxygen OI, which is conducive to the partial oxidation of CH_4 to produce syngas, tends to increase with the

Table 2. Surface atomic ratio for the samples measured by XPS

Oxygen carriers ($LaMn_xFe_{1-x}O_3$)	Surface compositions/%					
	Fe^{3+}/Fe_{total}	Mn^{3+}/Mn^{4+}	OI	OII	OIII	OI/(OI+OII+OIII)
x=0	37.23/62.77	-	27.3	17.1	27.7	37.86%
x=0.3	47.66/52.34	68.83/31.17	38.19	19.93	11.16	55.12%
x=0.5	52.79/47.21	71.27/28.73	40.82	14.07	12.57	60.51%
x=0.7	59.25/40.75	73.03/26.97	39.29	18.65	9.64	58.14%
x=1.0	-	71.22/28.78	40.05	14.77	14.71	57.60%

increase of Mn substitution, and get the maximum for the sample with x=0.5. It means that the proper substitution of Mn for Fe has a positive effect on the reactivity of $LaFe_{1-x}Mn_xO_3$ oxides for CH_4 partial oxidation. These results are also well-matched with the result by Mihai [24], who explained the chemical looping process by a kinetic study through varying the O content and the crystal size. In their opinion, the partial oxidation of methane was caused by the metal active site with the low coordinated oxygen on the

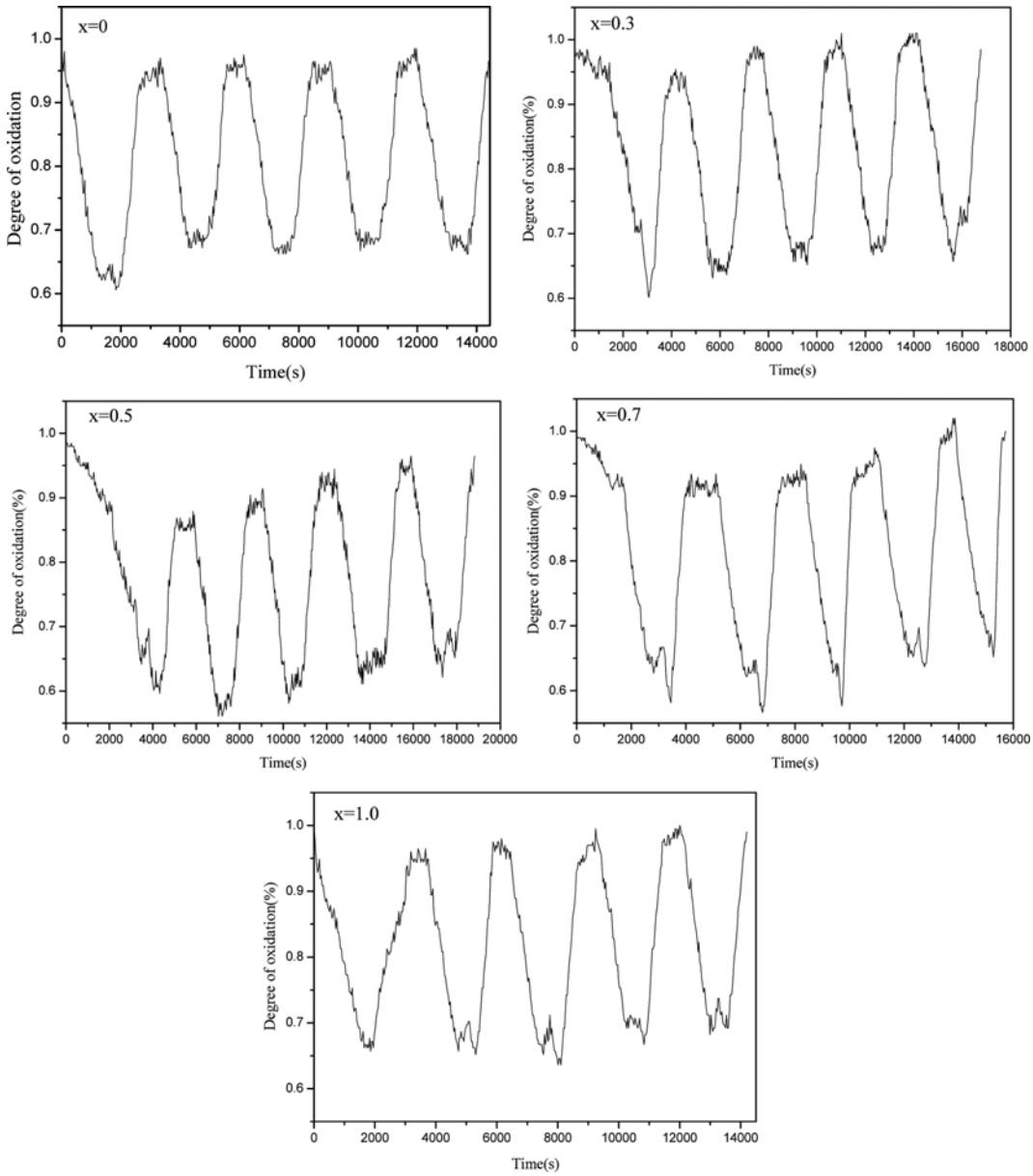

Fig. 6. Degree of oxidation as a function of reaction time in five cycles.

surface of the oxygen carrier. This site was prone to be generated when the oxygen mobility from the bulk to the surface was relatively low. However, the low oxygen mobility also gave rise to the methane decomposition, which caused the carbon formation. Therefore, there is the optimum oxygen mobility for the chemical looping methane partial oxidation. Besides, larger crystal has a high

Table 3. Degree of oxidation for oxygen carriers in cyclic reaction

$LaFe_{1-x}Mn_xO_3$ oxides	Reaction time	Cyclic number									
		1		2		3		4		5	
		X_{red}	X_{ox}	X_{red}	X_{ox}	X_{red}	X_{ox}	X_{red}	X_{ox}	X_{red}	X_{ox}
x=0	14430	0.60	0.95	0.65	0.96	0.65	0.95	0.65	0.95	0.65	0.95
x=0.3	16770	0.60	0.95	0.63	0.99	0.62	0.99	0.66	1.00	0.66	0.98
x=0.5	18810	0.60	0.86	0.56	0.90	0.58	0.94	0.61	0.94	0.64	0.96
x=0.7	15720	0.62	0.92	0.62	0.93	0.62	0.94	0.65	0.99	0.67	1.00
x=1.0	14190	0.67	0.96	0.66	0.97	0.65	0.94	0.69	0.98	0.70	0.99

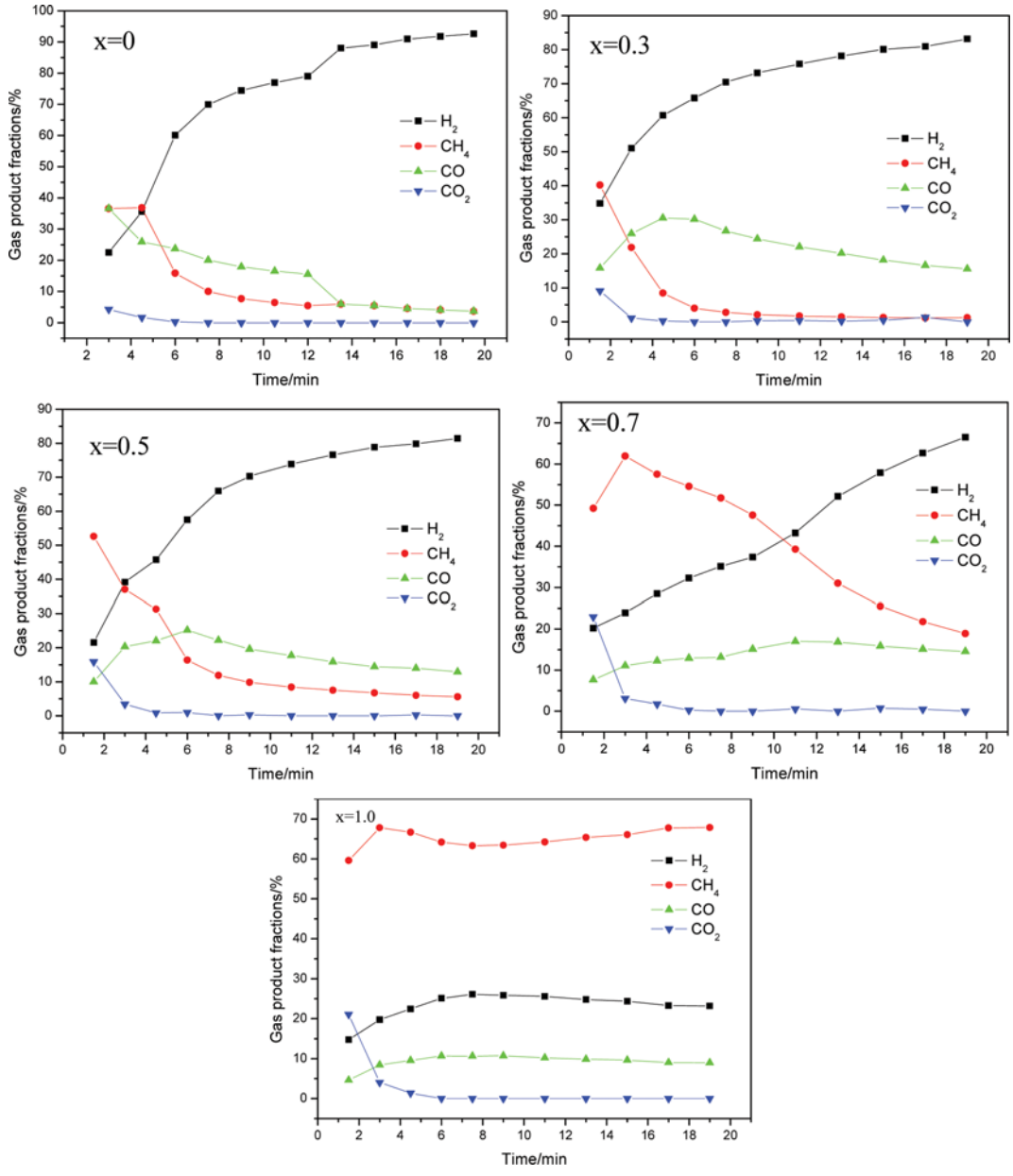

Fig. 7. Gas production fractions as a function of time during methane oxidation reactions.

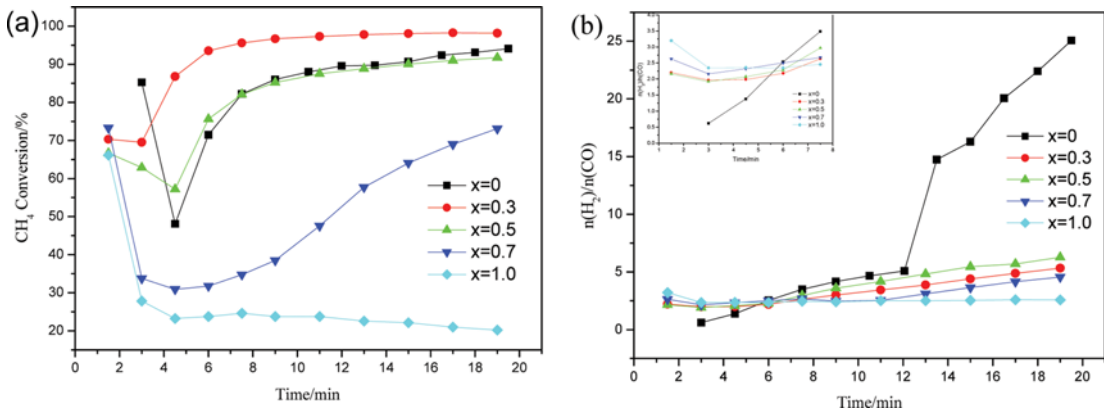

Fig. 8. Catalytic performance of oxygen carriers for methane selective oxidation. (a) CH_4 conversion, (b) H_2/CO ratio.

selectivity to synthesizing gas. The crystal sizes of the five perovskites were 16 nm, 13 nm, 28 nm, 8 nm and 5 nm, respectively, according to the XRD results. Consistent with these, the optimum value of Mn substitution was x=0.3-0.5 in $LaMn_xFe_{1-x}O_3$.

2. TGA Redox Reactivity

The degree of oxidation X as a function of time of $LaFe_{1-x}Mn_xO_3$ during the TGA redox experiments is shown in Fig. 6. The oxidation degrees of all the oxides decrease fast when exposed to CH_4 atmosphere, and finally decrease to about 0.6. It means that approximately 40% of the reactive oxygen took part into the reaction with CH_4. Note that the oxidation degree X shows a little increase after constantly decreasing, ascribed to the decomposition of CH_4 as the lattice oxygen species depleted. When the reacting atmosphere shifted to air, the oxidation degrees increased quickly due to the recovery of the oxygen, showing good regenerability. But the oxidation degree of X could not totally recover to 1.0, partly because of the departed adsorbed oxygen. Table 2 gives the detailed parameters of the redox process. The average degree of oxidation in the reduced form (Xred) was 0.64, 0.63, 0.60, 0.64 and 0.67 for $LaMn_xFe_{1-x}O_3$ with x=0, 0.3, 0.5, 0.7 and 1.0, respectively. Thus, 36%, 37%, 40%, 36%, and 33% of the active oxygen took part in the reaction of methane reduction. The amount of active oxygen which can be used in the methane reforming reaction for the oxygen carriers is in the order of: $LaFe_{0.5}Mn_{0.5}O_3$>$LaFe_{0.7}Mn_{0.3}O_3$>$LaFe_{0.3}Mn_{0.7}O_3$=$LaFeO_3$>$LaMnO_3$. $LaFe_{1-x}Mn_xO_3$ samples display good reduction property in methane reduction stage and regenerability in air oxidation stage. A proper substitution of manganese for iron improves the quantity of active oxygen in the oxides $LaFe_{1-x}Mn_xO_3$.

3. Fixed-bed Reaction Tests

Fig. 7 represents the gas product composition as a function of time which was conducted in a fixed bed reactor. High CO_2 concentrations were obtained at the initial stage of reaction with little fractions of CO and H_2. The sample with x=0 presents the lowest CO_2 fraction (under 5%), while the samples with x=0.3 and x=0.5 give CO_2 fractions around 10%. For the high degree of Mn substitution with x=0.7 and x=1.0, the CO_2 fractions are high up to 20% at the beginning of the reaction. These results are corresponding to the relative contents of adsorbed oxygen, which are shown in Table 1, considering the adsorbed oxygen is inclined to the CH_4 total oxidation to produce CO_2 and H_2O. Then the CO_2 fractions decreased sharply and closed to zero after the 6th minute as the reaction proceeded to consume the surface oxygen. Whereas, the CO and H_2 fractions increased continuously, attributed to the lattice oxygen which slightly lagged behind diffusing from the bulk to the surface to take part in the reaction. Meanwhile, methane decomposition that produced part of H_2 was another factor for the constantly increasing of H_2 fraction.

As important targets, methane conversion and H_2/CO molar ratio towards the reaction time at 850 °C for the $LaFe_{1-x}Mn_xO_3$ oxides, are shown in Fig. 8. For the samples with x=0, 0.3, 0.5 and 0.7, a high value of CH_4 conversions was observed at the initial stage. But it declined dramatically from the 2nd to 4th minute, and then increased rapidly thereafter. Finally, the CH_4 conversions reached 88%, 97.3% and 87.5% for the samples of $LaFeO_3$, $LaFe_{0.7}Mn_{0.3}O_3$ and $LaFe_{0.5}Mn_{0.5}O_3$, respectively. While the CH_4 conversion of $LaFe_{0.3}Mn_{0.7}O_3$ increased slowly and reached 73.1% finally at 19 min. The decline of methane conversion at 2nd to 4th min could be ascribed to the quick consumption of surface absorbed oxygen and the slight lagging of the lattice oxygen. $LaMnO_3$ shows a different pattern of methane conversion from other four kinds of oxides. The methane conversion on $LaMnO_3$ decreased continually and stayed at about 20% from 5 min to 19 min. During the process of CL-SMR, partial oxidation of methane and decomposition of methane were the two decisive factors for the methane conversion. It can be seen from Fig. 8(b), the sample $LaFeO_3$ gave high H_2/CO molar ratio far exceeding 2 : 1 after 12 min. It means that the higher CH_4 conversion of $LaFeO_3$ was largely attributed to methane cracking. The other four samples exhibit similar profiles of H_2/CO molar ratios, which are close to 2 : 1 in the dominating stage of the reaction. A more detailed graph of H_2/CO molar ratios from 1 min to 8 min is shown in the upper left area in the Fig. 8(b). The H_2/CO molar ratio of $LaFe_{0.7}Mn_{0.3}O_3$ and $LaFe_{0.5}Mn_{0.5}O_3$ stays relatively stable at the ideal value of 2.0 with little methane cracking, while those for the samples with x=0.7 and 1.0 exhibit unsuited value around 2.5. Therefore, an optimal range of the degree of Mn substitution is x=0.3-0.5 judging from the points of methane conversion and resistance to carbon formation.

4. Carbon Formation

Carbon formation from methane decompose is a negative factor in CL-SMR, which leads to the deactivation of oxygen carrier

and incomplete fuel utilization. Also, it is harmful for the steam oxidation stage because CO and CO_2 can be formed by the oxidation of carbon with steam, which decreases the purity of H_2. In the present experimental conditions, CH_4 conversion is attributed to partial oxidation of methane, as well as total oxidation of methane and methane cracking. Several likelihoods have to be considered to analyze the observed results:

$$\delta_1 CH_4 + LaFe_{1-x}Mn_xO_3 \rightarrow \delta_1 CO + 2\delta_1 H_2 + LaMn_xFe_{1-x}O_{3-\delta 1} \quad (2)$$

$$\delta_2/4CH_4 + LaFe_{1-x}Mn_xO_3 \rightarrow \delta_2/4CO_2 + \delta_1/2H_2O + LaFe_{1-x}Mn_xO_{3-\delta 2} \quad (3)$$

$$\delta_3 H_2 + LaFe_{1-x}Mn_xO_3 \rightarrow \delta_3 H_2O + LaFe_{1-x}Mn_xO_{3-\delta 3} \quad (4)$$

$$C + H_2O \rightarrow CO + H_2 \quad (5)$$

$$CO + H_2O \rightarrow CO_2 + H_2 \quad (6)$$

$$CH_4 \rightarrow C + 2H_2 \quad (7)$$

When methane was introduced into reactor, CO_2 and H_2O generated immediately according to reaction (3). As the reaction proceeded, reaction (2) of $LaFe_{1-x}Mn_xO_3$ with lattice oxygen dominated to produce H_2 and CO. With the continuous exhausting of oxygen in the oxide, methane decomposition happened as reaction (7). Methane decomposition mainly occurred at the later stage of reaction when the lattice oxygen was depleted, so reactions (5) and (6) were less frequent. For $LaFeO_3$, the H_2/CO ratio was far exceeding 2.0 at the later stage of the reaction, which indicates that reaction (7) was the main occurring reaction. While the samples with Mn substitution of $LaFe_{1-x}Mn_xO_3$ (x=0.3, 0.5, 0.7, 1.0) exhibited less carbon formation. Fig. 9 shows the H_2 generation and coke formation during the steam oxidation stage. The coke formation was calculated on the assumption that all the coke reacted with steam, and the CO and CO_2 generated in the steam oxidation stage were coming from coke. The hydrogen generation capacity of $LaFeO_3$ was the highest with 6.59 mmol per gram oxygen carrier. Accordingly, it produced the maximum coke by CH_4 decomposition, indicating a part of H_2 generation was caused by the steam gasification of carbon. While the hydrogen generation capacity for $LaFe_{0.7}Mn_{0.3}O_3$ and $LaFe_{0.5}Mn_{0.5}O_3$ was 4.86 and 4.04 mmol per gram oxygen carrier, respectively. Meanwhile, the coke formations of these two kinds of oxygen carriers exhibit moderate values. Another two kinds of oxygen carriers with high substitution of Mn, $LaFe_{0.3}Mn_{0.7}O_3$ and $LaMnO_3$ are not suitable for the CL-SMR on account of high methane decomposing and low H_2 generation capacity. By comparing the results of coke formation on the five kinds of oxygen carriers, it can be concluded that the Mn substitution in perovskite-type oxides $LaFe_{1-x}Mn_xO_3$ can reduce the amount of coke formation. But excessive Mn substitution (x>0.5) is disadvantageous for the hydrogen generation by fewer oxygen vacancy formation.

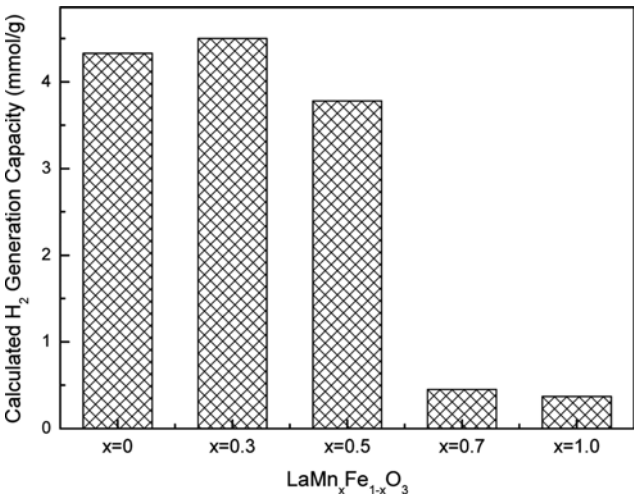

Fig. 10. Calculated H_2 generation capacity in steam oxidation step of $LaFe_{1-x}Mn_xO_3$ oxides.

Moreover, reactions (5) and (6) are another source for hydrogen generation in the steam oxidation step, and these parts of hydrogen cannot represent the authentic hydrogen generation capacity of $LaFe_{1-x}Mn_xO_3$. The calculated hydrogen amount generated by $LaFe_{1-x}Mn_xO_3$ oxides is shown in Fig. 10. $LaFe_{0.7}Mn_{0.3}O_3$ exhibits the highest hydrogen generation capacity with 4.5 mmol per oxygen carrier by deducting the influence of coke which was formed by CH_4 crack. The hydrogen generation capacity may be ranked in order of $LaFe_{0.7}Mn_{0.3}O_3$>$LaFeO_3$>$LaFe_{0.5}Mn_{0.5}O_3$>$LaFe_{0.3}Mn_{0.7}O_3$> $LaMnO_3$. That means substitution of Mn in perovskite type oxide has a positive effect on the resistance to coke formation. Meanwhile, Mn substitution could promote the reactivity of steam split-

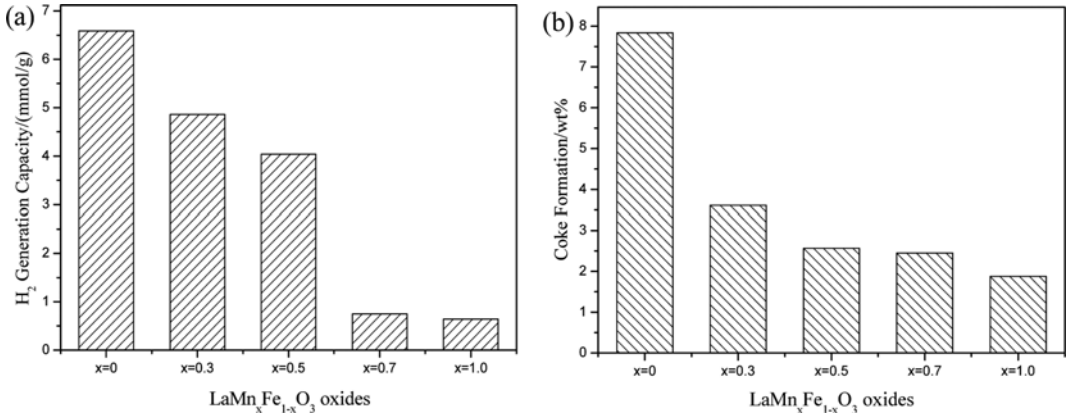

Fig. 9. Results of steam oxidation on the samples after CH_4 reduction. (a) H_2 generation capacity, (b) coke formation.

ting to produce hydrogen of the perovskites.

CONCLUSIONS

The desired monophasic crystalline perovskite phases were formed for $LaFe_{1-x}Mn_xO_3$ with different Mn substitution. The TPR patterns of $LaFe_{1-x}Mn_xO_3$ (x=0.3, 0.5, 0.7 and 1.0) presented a single reduction peak, indicating the simultaneous reduction of surface oxygen and bulk oxygen without clear distinction. Moreover, the reduction peak area that represents the hydrogen consumption increased as the degree of Mn substitution increased, indicating that the substitution of Mn for Fe could enhance the oxygen mobility from the bulk to the surface of the oxygen carrier particles. A mixed state of Mn^{3+} and Mn^{4+} existed in the $LaFe_{1-x}Mn_xO_3$ oxides, inducing the state of the iron element existence in the form of a mixture of Fe^{2+}, Fe^{3+} and Fe^{4+} in the Mn-doped perovskite. The optimal range of the degree of Mn substitution is x=0.3-0.5 judging from the multicyclic TG redox reaction, CH_4 conversion and molar ratio of H_2/CO. In the steam oxidation stage, the hydrogen generation capacity is 4.86 and 4.04 mmol per gram oxygen carrier for $LaFe_{0.7}Mn_{0.3}O_3$ and $LaFe_{0.5}Mn_{0.5}O_3$, with less coke formation. $LaFe_{0.3}Mn_{0.7}O_3$ and $LaMnO_3$ with high substitution of Mn are not suitable for the CL-SMR due to high methane decomposition and low H_2 generation capacity.

ACKNOWLEDGEMENTS

This work was supported by the National Natural Science Foundation of China (51406208, 51406214). We acknowledge the Science & Technology Research Project of Guangdong Province (2015A010106009). We also thank the support of Key Laboratory of Renewable Energy, Chinese Academy of Sciences (Y607j51001).

REFERENCES

1. K. Z. Li, H. Wang, Y. G. Wei and D. X. Yan, *Chem. Eng. J.*, **156**, 512 (2010).
2. K. Otsuka, T. Ushiyama and I. Yamanaka, *Chem. Lett.*, **9**, 1517 (1993).
3. H. J. Richter and K. F. Knoche, *ACS Symp. Ser.*, **235**, 71 (1983).
4. K. Z. Li, H. Wang and Y. G. Wei, Syngas Generation from Methane Using a Chemical-Looping Concept: A Review of Oxygen Carriers, J. Chem. 2013, Article ID 294817, 8 pages.
5. X. P. Dai, R. J. Li, C. C. Yu and Z. P. Hao, *J. Phy. Chem. B*, **110**, 22525 (2006).
6. R. J. Li, C. C. Yu, X. P. Dai and S. K. Shen, *Chin. J. Cata.*, **23**, 549 (2002).
7. M. Rydén, A. Lyngfelt, T. Mattisson, D. Chen, A. Holmen and E. Bjørgum, *Int. J. Greenh. Gas. Con.*, **2**, 21 (2008).
8. L. Nalbanidian, A. Evdou and V. Zaspalis, *Int. J. Hydrogen Energy*, **34**, 7162 (2009).
9. V. García, M. T. Caldes, O. Joubert, E. Gautron, F. Mondragón and A. Moreno, *Catal. Today*, **157**, 177 (2010).
10. L. Nalbandian, A. Evdou and V. Zaspalis, *Int. J. Hydrogen Energy*, **36**, 6657 (2011).
11. L. M. Neal, A. Shafiefarhood, F. X. Li, *ACS Catal.*, **4**, 3560 (2014).
12. H. S. Lim, D. Kang and J. W. Lee, *Appl. Catal. B: Environ.*, **202**, 175 (2017).
13. M. Rydén, H. Leion, T. Mattisson and A. Lyngfelt, *Appl. Energy*, **113**, 1924 (2014).
14. G. Azimi, H. Leion, M. Ryden, T. Mattisson and A. Lyngfelt, *Energy Fuels*, **27**, 367 (2013).
15. H. J. Wei, Y. Cao, W. J. Ji and C. T. Au, *Catal. Commun.*, **9**, 2509 (2008).
16. F. He, X. A. Li, K. Zhao, Z. Huang, G. Q. Wei and H. B. Li, *Fuel*, **108**, 465 (2013).
17. K. Zhao, F. He, Z. Huang, G. Q. Wei, A. Q. Zheng, H. B. Li and Z. Z. Zhao, *Appl. Energy*, **168**, 193 (2016).
18. J. D. Li, G. S. Luo, G. W. Jiang, W. S. Li and Z. Y. Zhou, *J. Nanchang University*, **34**, 279 (2010).
19. S. Jauhar, M. Dhiman, S. Bansal and S. Singhal, *J. Sol. Gel. Sci. Technol.*, **75**, 124 (2015).
20. I. Atribak, L. A. Bueno and G. A. Garcia, *J. Catal.*, **259**, 123 (2008).
21. H. K Wang, P. C. Dong, J. S. Bae, S. Adams and V. Thangadurai, *Solid State Ionics*, **290**, 90 (2016).
22. K. Tabata, Y. Hirano and E. Suzuki, *Appl. Catal. A: Gen.*, **170**, 245 (1998).
23. X. Li, H. B. Zhang, X. X. Liu, S. J. Li and M. Y. Zhao, *Mater. Chem. Phys.*, **38**, 355 (1994).
24. O. Mihai, D. Chen and A. Holmen, *J. Catal.*, **293**, 175 (2012).